Organic LETTERS

Letter

pubs.acs.org/OrgLett

Synthesis and Structural Analysis of Thiophene-Pyrrole-Based *S,N*-Heteroacenes

Christoph Wetzel,[†] Amaresh Mishra,[†] Elena Mena-Osteritz,[†] Andreas Liess,[‡] Matthias Stolte,[‡] Frank Würthner,[‡] and Peter Bäuerle*,[†]

[†]Institut für Organische Chemie II und Neue Materialien, Universität Ulm, Albert-Einstein-Allee 11, 89081 Ulm, Germany

[‡]Institut für Organische Chemie & Center for Nanosystems Chemistry, Universität Würzburg, Am Hubland, 97074 Würzburg, Germany

Supporting Information

ABSTRACT: Fused *S,N*-heterohexacene **4** was synthesized by applying Pd-catalyzed tandem Buchwald–Hartwig coupling and further functionalized to corresponding acceptor-capped derivatives **5** and **6** showing bond length equalization in the π-conjugated backbone and intense optical transitions. Organic thin film transistors (OTFTs) based on a vacuum-deposited film of **6** exhibit p-channel charge-carrier mobilities as high as 0.021 $cm^2\ V^{-1}\ s^{-1}$ and current on/off ratios of 10^5.

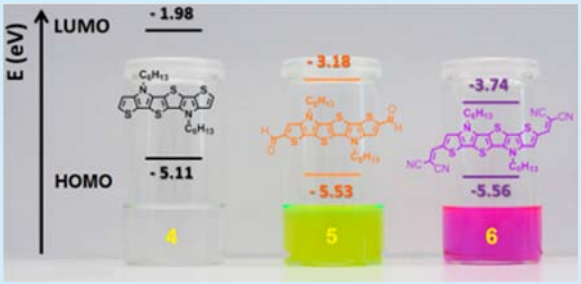

Over the past decade, there has been remarkable development in the field of acenes for organic electronics.[1] Among them, pentacene and its derivatives show outstanding charge carrier mobilities up to 40 $cm^2\ V^{-1}\ s^{-1}$.[1a] Higher acenes such as hexa- or heptacene were synthesized, although they become increasingly instable because of destabilization of the HOMO energy level and therefore have only limited applicability.[2] In comparison to pentacene, stabilization of the HOMO energies can be achieved by implementation of heteroatoms, e.g., in *N*-heteroacenes[3] (ΔE = 0.3–1 eV) or by fusion of thiophene rings in thienoacenes (ΔE = 0.67 eV).[1b,4,5] The incorporation of heteroatoms allows for fine-tuning of their electronic properties and specific intermolecular interactions in the solid state. In thienoacenes the molecular packing changes from herringbone to π-stacking structure due to reduced C–H$\cdots\pi$ interactions.[1a,6]

The first synthesis of pentathienoacene suffered from low yields and hindered accessibility to longer thienoacenes due to low solubility of the precursors.[7] Recently, penta- and hexathienoacenes were synthesized in moderate isolated yields of about 25 and 6%, respectively.[5] Matzger et al. reported an improved route by introducing terminal triisopropylsilyl groups to enhance the solubility of the precursors.[8] Penta- and heptathienoacenes were isolated with yields of 70–80%; however, they showed very low solubility due to the absence of any alkyl side chains.

We report here synthesis and characterization of novel *S,N*-heterohexacene (SN6) **4** and its acceptor-capped derivatives **5** and **6**, which show strong intermolecular interactions and dense packing in the solid state, are thermally stable, and exhibit strong absorption at low energy in the visible spectrum. The structural construction principle of our SN6 oligomers leads to an extended band-like conjugated π-system of seven conjugated double bonds, which according to calculations and X-ray data, comprises substantial quinoidal character and bond length equalization in the ground state (vide infra). Our SN6 basic system **4** can be regarded as a structural extension to dithieno[3,2-*b*:2′,3′-*d*]pyrrole (DTP) and dithieno[2,3-*d*:2′,3′-*d*′]thieno[3,2-*b*:4,5-*b*′]dipyrrole (SN5) reported by Rasmussen et al.[9] and Suga et al.,[10] respectively. Structure–property relationships and first charge transport data of these novel organic semiconductors will be presented.

Synthesis started from 3,6-dibromo-2,5-bis(3-bromothien-2-yl)thieno[3,2-*b*]thiophene **3**, which was obtained as central building block by Pd-catalyzed coupling of metalated 2,3-dibromothiophene **1** and tetrabromothieno[3,2-b]thiophene **2**. Tandem Buchwald–Hartwig reaction of tetrabromide **3** with 1-hexylamine gave ring-fused *S,N*-heterohexacene **4** in 54% yield. Subsequent Vilsmeier–Haack formylation of **4** gave dialdehyde **5** in 80% yield, which by Knoevenagel condensation with malononitrile provided the dicyanovinylene (DCV)-capped SN6 derivative **6** (Scheme 1). All compounds were characterized by NMR and HRMS spectral analysis to prove the structures (see Supporting Information (SI)).

SN6 basic system **4** crystallizes in the monoclinic space group $P2_1/n$ with two equivalent molecules in the unit cell arranging in a 2-fold screw axis symmetry (a = 5.0953(9), b = 26.540(5), c = 8.7806(16) Å; α = 90.00, β = 95.669(4), γ = 90.00°). Bond lengths, angles, and torsion angles are compiled in Table S1 (SI). The alkyl chains direct out of the plane of the perfectly planar conjugated backbone (Figures 1a and S1 (SI)). The

Received: November 1, 2013
Published: December 20, 2013

dx.doi.org/10.1021/ol403153z | *Org. Lett.* 2014, 16, 362–365

Scheme 1

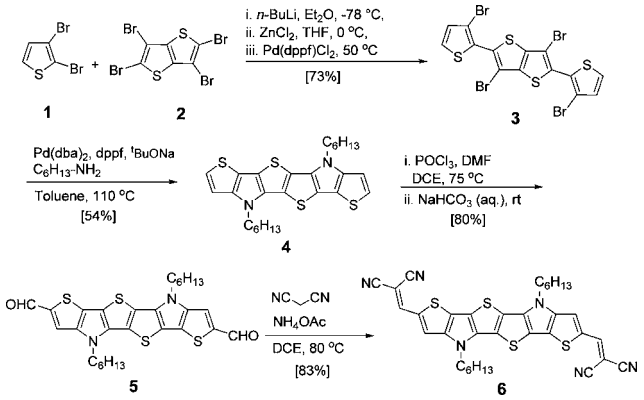

molecules of **4** order in columns via $\pi-\pi$ interaction at distances of 3.37 Å. A strong interaction between the columns is provided by S−S dipolar forces at distances of 3.55 Å, far below the van der Waals radii (Figure 1b, red and green lines; Tables S2 and S3 (SI)).

Dialdehyde **5** crystallizes in the triclinic space group $P\bar{1}$ with two nonequivalent molecules in the unit cell (a = 4.84737(17), b = 16.2215(6), c = 16.7511(5) Å; α = 86.998(3), β = 81.961(3), γ = 84.851(3)°). The two molecules exhibit slight differences in the conjugated backbone and a more evident deviation in the arrangement of the alkyl chains (Figures S3 (SI) and 1c, dashed romboids and arrows). SN6 **5** orders in planes, in which the molecules form a quasi-hexagonal packing driven by multiple interactions of the terminal aldehyde groups (Figure 1c, cyan lines; Table S5 (SI)). The layered structure evidenced interplane distances of 3.5 Å and closest $\pi-\pi$ interaction through the aldehyde C16-βC8 thiophene at a distance of 3.27 Å (Table S5 (SI); Figure 1d, red and green lines) in spite of the presence of alkyl chains in between the planes. In comparison to the SN6 basic system **4**, the aldehyde groups in **5** are responsible for the bond-length equilibration in the carbon backbone (vide infra) (see Tables S1 and S4 (SI)).

The thermal stability of the SN6 derivatives was investigated by differential scanning calorimetry (DSC). The melting points increase from 163 °C for **4** to 319 °C for **5**, and 366 °C for **6**. The onset of decomposition temperature (T_d) for derivatives **5** and **6** were 338 and 370 °C, respectively, giving a high thermal stability (Figure S3 (SI)).

The optical properties of the novel SN6-hexacenes **4**−**6** were investigated by UV−vis and fluorescence spectroscopy (Figure 2; Table 1). Parent system SN6 **4** showed highly structured absorption bands at high (λ_{max} = 326, 313, and shoulder at 300 nm) and low energies (λ_{max} = 380, 362, and shoulder at 345 nm). The latter band can be attributed to a $\pi-\pi^*$ electronic transition, in which the multiple vibronic splitting originates from the rigidity of the conjugated π-system.

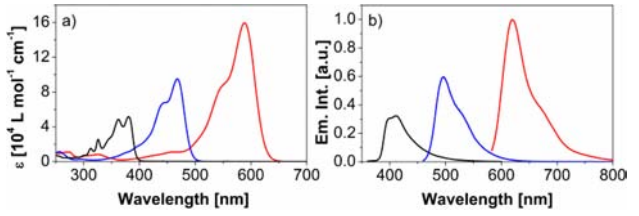

Figure 2. UV−vis absorption (a) and fluorescence spectra (b) of SN6 oligomers **4** (black), **5** (blue), and **6** (red) in dichloromethane solution.

These absorption bands of SN6 **4** are red-shifted in comparison to the shorter homologues SN5[10] and DTP-butyl,[9a] which is explained by the extension of the conjugated backbone. The absorption data well matches to this of hexathienoacene (S6) (λ_{max} = 324, 380 nm) indicating no differences after nitrogen-by-sulfur substitution.[7] The emission of SN6 **4** had a maximum at 411 nm with a shoulder at ca. 398 nm and is comparable to this of S6 (416 nm).[7] Because of the rigid structural backbone a Stokes shift of only 898 cm^{-1} is observed, indicating a similar geometry in the ground and the first excited state.

The insertion of terminal acceptor groups to the parent SN6 **4** significantly red-shifted the lower energy absorption band to 468 nm for **5** and to 588 nm for **6**, which evidence less prominent vibronic splitting.

Simultaneously, the molar extinction coefficients drastically increase and the optical energy gaps E_g^{opt} decrease. The emissions of SN6 **5** and **6** were expectedly as well red-shifted to 496 and 620 nm giving rise to relatively small Stokes shifts.

The optical data reveal that the HOMO → LUMO gap of the SN6 derivatives **5** and **6** decreases as a consequence of both the elongated π-system and the significant degree of intramolecular charge transfer from the rigid donor backbone to the terminal electron-accepting aldehyde or DCV units. These trends in absorption behavior were corroborated by density functional theory calculations (vide infra).

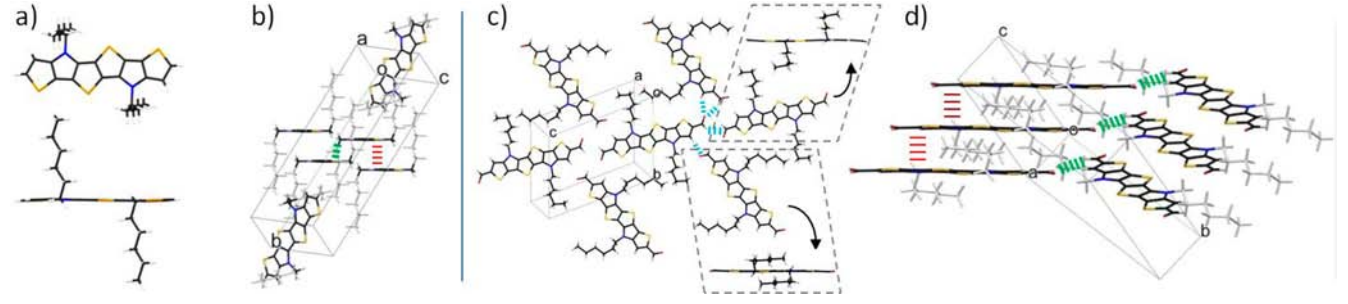

Figure 1. Single crystal X-ray structure analysis of hexyl-substituted SN6 **4**, individual molecule on the (8 48 −2) plane and perpendicular to (a), top and bottom, respectively, and packing in the unit cell (b). Single crystal X-ray structure analysis of dialdehyde **5**, packing in the (3 10 −3) plane including the two molecules in the unit cell (dashed romboids) and their perpendicular view (c). Layered packing motif perpendicular to the (3 10 −3) plane (d). Alkyl chains have been softened up for clarity in (b) and (d).

dx.doi.org/10.1021/ol403153z | Org. Lett. 2014, 16, 362−365

Table 1. Summary of Optical and Electrochemical Properties of SN6 Derivatives 4−6

SN6	λ_{abs} [nm][a]	ε [L mol^{-1} cm^{-1}]	λ_{em} [nm][a]	E_g^{opt} [eV][b]	ΔE_S [cm^{-1}][c]	E°_{ox1} [V]	E°_{ox2} [V]	E°_{red1} [V]	HOMO [eV][d]	LUMO [eV][d]	E_g^{CV} [eV][f]
4	326, 380	51600	411	3.15	898	0.06	0.73	—	−5.11	−1.96[e]	3.15
5	468	95200	496	2.52	788	0.50	1.03	−1.98	−5.51	−3.18	2.33
6	588	159600	620	1.98	649	0.57	1.09	−1.49	−5.56	−3.74	1.82

[a]Measured in dichloromethane solution. [b]Estimated using the onset of the UV−vis spectrum in solution by $E_g^{opt} = 1240/\lambda_{onset}$. [c]Stokes shift. [d]Estimated from the onset of the respective redox waves, Fc/Fc^+ value set to −5.1 eV vs vacuum. [e]Determined from the optical band gap and HOMO. [f]Calculated from $E_g = E_{LUMO} - E_{HOMO}$.

The redox behavior of the SN6-oligomers **4**−**6** was investigated using cyclic voltammetry (Figure S4 (SI)). Typical first and second reversible oxidations were found at E°_{ox1} = 0.06 V and E°_{ox2} = 0.73 V vs Fc/Fc^+ characteristic for the formation of stable radical cations and dications of SN6 **4**. The introduction of acceptor groups of increasing strength in **5** and **6** resulted in a gradual positive shift of the oxidation potentials to 0.50 and 1.03 V for **5** and to 0.57 and 1.09 V for **6**. The reduction waves at −1.98 V for **5** and −1.49 V for **6** related to the simultaneous one-electron transfer to the acceptor groups become visible. The HOMO energies of the SN6 derivatives, which were determined from the onsets of the respective oxidation waves, decrease from **4** (−5.11 eV) to **5** (−5.51 eV) and **6** (−5.56 eV). The LUMOs, however, are continuously destabilized on going from **4** (−1.96 eV) to **5** (−3.18 eV) and to **6** (−3.74 eV) leading to a decreasing electrochemical gap E_g^{CV} according to the increasing acceptor strength.

Quantum chemical DFT calculations on SN6 **4**−**6** allow for the description of the frontier orbitals (Figure 3). In contrast to the nonfused systems, in which the coefficients of the sulfur atoms to the HOMO are negligible,[11] the electron density distribution in the HOMO of the fused systems showed a noticeably contribution of the S and N heteroatoms. In all cases the LUMO exhibits the classical quinoidal character with the electron density partially localized on the acceptor groups (Figure 3). The first electronic transition, which is calculated to be predominantly HOMO → LUMO (vide infra) in the case of **5** and **6** leads to a low-energy absorption with CT character.

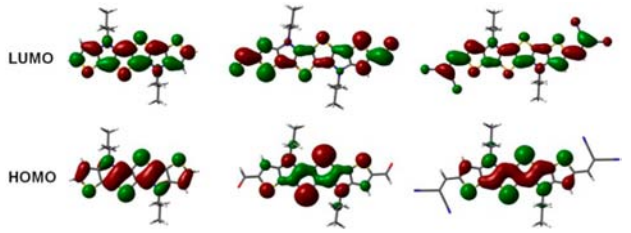

Figure 3. HOMO/LUMO electron density distribution of SN6 **4** (left) and acceptor-substituted SN6 **5** (middle) and **6** (right).

In contrast to the classical nodal HOMO distribution in the conjugated backbone of **4**, the HOMOs of derivatives **5** and **6** evidence an intriguing continuous electron density in the inner π-conjugated system (Figure 4). The calculated bond length alternation (BLA), $\langle\Delta r\rangle$, is reduced from 0.025 to 0.018 and 0.012 on going from **4**−**6**. This trend well correlates with the data obtained from X-ray crystal structure analysis, where the BLA is even smaller (**4**: 0.017, **5**: 0.0045). We can therefore conclude that the acceptor substitution in our *S,N*-heteroacenes leads to a bond equilibration toward the cyanine limit.[12] Consistently, the electron density distribution in the HOMO of **5** denotes no nodes in the internal carbon backbone as a consequence of the two equally canonical resonance structures contributing to the ground state configuration of the molecule.

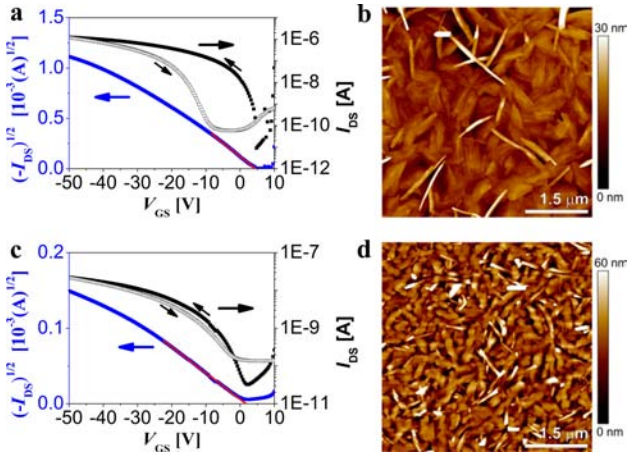

Figure 4. OTFT transfer curves of SN6 **6** on (a) OTES-modified substrate and (b) corresponding AFM image; on (c) bare Si/SiO_2 and (d) corresponding AFM image.

To demonstrate the suitability of the SN6 π-system for applications in organic electronics, bottom-gate, top-contact TFTs were prepared by vacuum sublimation. Accordingly, SN6 **6** was deposited as active layer on bare and on *n*-octadecyltriethoxysilane (OTES) treated Si/SiO_2 (100 nm) substrates. The details for device fabrication and characterization are given in Table S7 (SI). Typical transfer curves on OTES-modified and bare Si/SiO_2 substrates for devices operating under ambient conditions in the saturation regime (V_{DS} = −50 V) are depicted in Figure 4a,c. Hole mobilities ($\mu_{p,max}$) as high as 3.5×10^{-4} cm^2 V^{-1} s^{-1} on Si/SiO_2 and 2.1×10^{-2} cm^2 V^{-1} s^{-1} on OTES-modified substrate, respectively, were deduced from the slope of the square root of the drain current $(I_{DS})^{1/2}$ vs the gate voltage (V_{GS}) for TFTs when the oligomer was deposited at an optimized substrate temperature of 160 °C. The difference in charge carrier mobilities on different substrates was rationalized by atomic force microscopy (AFM) showing a better lamellar growth (layer heights of 1.3 ± 0.1 nm) and larger grains for the OTES-modified substrate (Figure 4b,d). Current on/off ratios (I_{on}/I_{off}) were determined to be in the order of 10^3 and 10^5, respectively. The mobilities of **6** on OTES-modified substrates are remarkably high in comparison to DCV4T (10^{-4} cm^2 V^{-1} s^{-1})[13] and to thienohexacene S6 (6×10^{-3} cm^2 V^{-1} s^{-1}),[7] considering the small size and molecular rigidity of the π-conjugated scaffold. For the OTFTs on OTES-modified substrate, there is a hysteresis in the transfer curve. The hysteresis decreases with consecutive measurements of the transfer characteristics as the threshold voltage (V_T) is shifted from 4 V (first measurement) toward negative values (−10 V, fifth measurement), while the hole mobility (2.3×10^{-2} cm^2 V^{-1} s^{-1}) and on/off ratio (2.5×10^5) stay unchanged.

dx.doi.org/10.1021/ol403153z | Org. Lett. 2014, 16, 362−365

In conclusion, in view of the demand of more stable longer acene systems, we have developed novel *S,N*-heterohexacenes **4**–**6** with an extended band-like structure by multiple fusion of thiophene rings through N–R bridges. Interesting structural features were elucidated by X-ray single crystal analysis, in which planar backbones and layered packing with strong π–π stacking interactions were found for **4** and **5**. The optoelectronic properties are governed by the planarity of the system and the electron delocalization. Thus, increasing intensitites and red-shifts in absorption and simultaneously decreasing energy gaps were found on going from **4** to **6**, well correlating with increasing acceptor strength. Theoretical calculations corroborate the pecularity of the novel π-systems by identifying bond-length equalization in the carbon backbone toward the cyanine limit. The small BLA, planarity, optoelectronic and good charge transport properties qualify the *S,N*-heteroacenes for application in organic electronics. Synthesis of higher *S,N*-heteroacenes is under way in our laboratory.

■ ASSOCIATED CONTENT

Supporting Information

Materials, syntheses, NMR, MS, DSC, and X-ray structure analysis details. This material is available free of charge via the Internet at http://pubs.acs.org.

■ AUTHOR INFORMATION

Corresponding Author

peter.baeuerle@uni-ulm.de

Notes

The authors declare no competing financial interest.

■ ACKNOWLEDGMENTS

The authors gratefully acknowledge financial support of the Federal Ministry of Education and Research (BMBF) in the frame of joint project (LOTsE, 03EK3505G) and Prof. M. Weil, University of Vienna, for providing the X-ray structure analysis measurements.

■ REFERENCES

(1) (a) Mei, J.; Diao, Y.; Appleton, A. L.; Fang, L.; Bao, Z. *J. Am. Chem. Soc.* **2013**, *135*, 6724–6746. (b) Jiang, W.; Li, Y.; Wang, Z. *Chem. Soc. Rev.* **2013**, *42*, 6113–6127. (c) Watanabe, M.; Chang, Y. J.; Liu, S.-W.; Chao, T.-H.; Goto, K.; Islam, M. M.; Yuan, C.-H.; Tao, Y.-T.; Shinmyozu, T.; Chow, T. J. *Nat. Chem.* **2012**, *4*, 574–578. (d) Anthony, J. E. *Chem. Rev.* **2006**, *106*, 5028–5048.

(2) (a) Einholz, R.; Bettinger, H. F. *Angew. Chem., Int. Ed.* **2013**, *53*, 9818–9820. (b) Zade, S. S.; Bendikov, M. J. *Phys. Org. Chem.* **2012**, *25*, 452–461. (c) Zade, S. S.; Bendikov, M. *Angew. Chem., Int. Ed.* **2010**, *49*, 4012–4015.

(3) Bunz, U. H. F.; Engelhart, J. U.; Lindner, B. D.; Schaffroth, M. *Angew. Chem., Int. Ed.* **2013**, *52*, 3810–3821.

(4) (a) Takimiya, K.; Shinamura, S.; Osaka, I.; Miyazaki, E. *Adv. Mater.* **2011**, *23*, 4347–4370. (b) Skabara, P. J. Fused oligothiophenes. In *Handbook of Thiophene-Based Materials*; Perepichka, I. F., Perepichka, D. F., Eds.; Wiley-VCH: Weinheim, 2009; Vol. *1*, pp 219–254.

(5) (a) Xiao, K.; Liu, Y.; Qi, T.; Zhang, W.; Wang, F.; Gao, J.; Qiu, W.; Ma, Y.; Cui, G.; Chen, S.; Zhan, X.; Yu, G.; Qin, J.; Hu, W.; Zhu, D. *J. Am. Chem. Soc.* **2005**, *127*, 13281–13286. (b) Liu, Y.; Sun, X.; Di, C.; Liu, Y.; Du, C.; Lu, K.; Ye, S.; Yu, G. *Chem.—Asian J.* **2010**, *5*, 1550–1554.

(6) (a) Brédas, J. L.; Calbert, J. P.; da Silva Filho, D. A.; Cornil, J. *Proc. Natl. Acad. Sci. U. S. A.* **2002**, *99*, 5804–5809. (b) Würthner, F.; Schmidt, R. *ChemPhysChem* **2006**, *7*, 793–797.

(7) Mazaki, Y.; Kobayashi, K. *Tetrahedron Lett.* **1989**, *30*, 3315–3318.

(8) Zhang, X.; Côté, A. P.; Matzger, A. J. *J. Am. Chem. Soc.* **2005**, *127*, 10502–10503.

(9) (a) Ogawa, K.; Rasmussen, S. C. *J. Org. Chem.* **2003**, *68*, 2921–2928. (b) Rasmussen, S. C.; Evenson, S. J. *Prog. Polym. Sci.* **2013**, *38*, 1773–1804.

(10) Mitsudo, K.; Shimohara, S.; Mizoguchi, J.; Mandai, H.; Suga, S. *Org. Lett.* **2012**, *14*, 2702–2705.

(11) Fitzner, R.; Reinold, E.; Mishra, A.; Mena-Osteritz, E.; Ziehlke, H.; Körner, C.; Leo, K.; Riede, M.; Weil, M.; Tsaryova, O.; Weiß, A.; Uhrich, C.; Pfeiffer, M.; Bäuerle, P. *Adv. Funct. Mat.* **2011**, *21*, 897–910.

(12) (a) Dähne, S.; Radeglia, R. *Tetrahedron* **1971**, *27*, 3673–3693. (b) Tolbert, L. M.; Zhao, X. *J. Am. Chem. Soc.* **1991**, *113*, 3253–3258. (c) Würthner, F.; Wortmann, R.; Matschiner, R.; Lukaszuk, K.; Meerholz, K.; DeNardin, Y.; Bittner, R.; Bräuchle, C.; Sens, R. *Angew. Chem., Int. Ed.* **1997**, *36*, 2765–2768.

(13) Schrader, M.; Fitzner, R.; Hein, M.; Elschner, C.; Baumeier, B.; Leo, K.; Riede, M.; Bäuerle, P.; Andrienko, D. *J. Am. Chem. Soc.* **2012**, *134*, 6052–6056.